High data density temperature measurement for quasi steady-state flows

C. R. Mercer, N. Rashidnia, K. Creath

Abstract A new optical instrument, the liquid crystal point diffraction interferometer (LCPDI), is used to measure the temperature distribution across a heated chamber filled with silicone oil. Data taken using the LCPDI are compared to equivalent measurements made with a traversing thermocouple and the two data sets show excellent agreement. This instrument maintains the compact, robust design of Linnik's point diffraction interferometer and adds to it phase stepping capability for quantitative interferogram analysis. The result is a compact, simple to align, environmentally insensitive interferometer capable of accurately measuring optical wavefronts with very high data density and with automated data reduction.

1
Introduction

The point diffraction interferometer (PDI) has long been used as a robust instrument for the measurement of optical wavefronts for lens testing and fluid flow diagnostics (Linnik 1933; Smartt and Strong 1972). The PDI is robust because it has a common-path design. Air turbulence and mechanical vibrations affect both the object and the reference beams in the same way. This makes the interferometer more robust than either Mach-Zender or Michelson interferometers, especially when measuring large objects like wind tunnel flows where the optical paths are very long. Still, reasonable care must be taken to limit mechanical vibrations because motion of the filter relative to the optical train will affect results. The common-path design has other advantages because relatively few optical elements are required. The cost, size, and weight of the instrument are low. Alignment is simple. These features also make the instrument attractive for remote applications like those found on SpaceLab.

Although it was implied long ago that the PDI would be useful for fluid studies (Linnik 1933), the PDI has not been widely used for this purpose. Qualitative demonstrations have been performed (Aggarwal and Kaura 1986; Giglio et al. 1987; Musazzi et al. 1993), and the PDI was selected for use as an instrument for fluid measurements on the International Microgravity Lab 2, but, like any interferometer used for complex fluid property measurements, quantitative results have been difficult to obtain. The reason for this is that the interferograms must be interpreted to extract information about the object wavefront. One method sometimes employed is manual fringe counting. This method is tedious, labor intensive, and subject to error, and so is not widely used. Alternatively fringe following software is available to automate this task. It works on the same principle as manual fringe counting: peaks or valleys of continuous interference fringes are identified. These lines represent lines of constant phase on the object beam wavefront. The wavefront is reconstructed successively adding or subtracting 2π radians to each line, and interpolating between lines. The accuracy of this method is limited by the ability to find the true peaks and valleys of the fringe. This task is difficult because the slope of a cosine at its peaks and valleys is zero. Also, the sign of the aberration can not be determined from a single interferogram. The PDI plate must be moved relative to the focused beam and the fringe motion observed to determine the sign (Speer et al. 1979).

The most accurate and effective way to measure both the magnitude and the sign of wavefront aberrations is to use phase shifting interferometry (PSI) (Bruning et al. 1974). The minimum number of required frames is 3, but more frames will improve the measurement by reducing the sensitivity to phase stepping errors. Standard algorithms are published for 3, 4, 5 and 6 frames (Greivenkamp and Bruning 1992). There are several assumptions common to all of these algorithms, namely that the intensities of the object and reference beams at each pixel do not vary from frame to frame, that the object phase remains constant during the entire acquisition time, and that the phase steps do not vary across the detector. The phase at each point in the interferogram is calculated independently, producing a phase map with at least as much spatial resolution as there are pixels in the recording device. To use this technique the interferometer must provide control over the relative phase of the object and reference beams.

This paper describes the use of a new point diffraction interferometer with a liquid crystal filter that permits arbitrary

C. R. Mercer
NASA Lewis Research Center,
Cleveland, OH 44135, USA

N. Rashidnia
NYMA, Inc., NASA LeRC
Cleveland, OH 44135, USA

K. Creath
University of Arizona, Optical Science Center,
Tucson, AZ 85721, USA

Correspondence to: C. R. Mercer

phase shifts to be introduced between the object and reference beams. A microsphere embedded within the liquid crystal layer provides a locally generated reference beam. The object beam is phase shifted by modulating the voltage across the liquid crystals, altering the refractive index of the birefringent nematic liquid crystals. This technique permits the use of phase shifting interferometry to analyze the interferograms, providing accurate, automated, high density data.

2
Liquid crystal PDI

The liquid crystal point diffraction interferometer (LCPDI) works in the same way as the classic PDI (Mercer and Creath 1994a). Light is brought to a focus on and is filtered by the PDI plate. The central portion of the incident wave is diffracted to form a spherical reference wave, while the remainder of the light travels through the filter with its information content intact, forming the object wave. Aberrations in the incident wave are indicated by the resultant interferogram.

The differences between the LCPDI and the PDI lie in the physical differences in the filter. The PDI uses a neutral density filter with a pinhole; the LCPDI uses a liquid crystal layer with an embedded microsphere. Phase modulation is achieved by manipulating the orientation of the individual molecules to control the refractive index of the liquid crystal layer. The phase of light passing through a hole in the layer will not be affected, so the phase difference between the object and reference beams can be controlled. This allows completely flexible phase stepping while retaining the full common-path optical design.

The LCPDI is shown schematically in Fig. 1. Nematic liquid crystals (LC) are sandwiched between two glass plates. Nine micron diameter cylindrical rods are placed at the edges of the plates to serve as spacers. Transparent plastic microspheres, nominally 9 μm in diameter, are scattered throughout the liquid crystal layer. Each microsphere replaces a small volume of liquid crystals as the filler between the glass plates. Dye is added to the liquid crystals to attenuate the object beam to
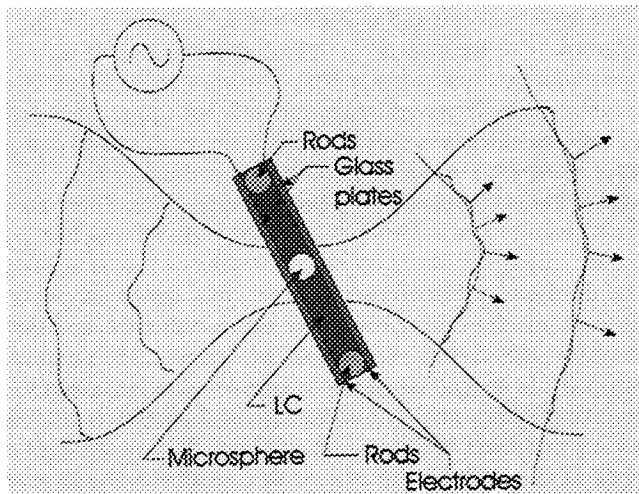
roughly the same intensity as the reference beam. This improves the fringe contrast, but the dye molecules rotate with the liquid crystal molecules causing an intensity modulation when the phase is shifted.

Transparent electrodes are deposited on the two plates' inner surfaces, and leads are soldered onto these electrodes so that an alternating current can be applied across the liquid crystal. Parallel microgrooves are etched into the electrodes so that the nematic liquid crystals are homogeneously aligned. When the field is applied, the liquid crystal dipoles realign themselves so that they rotate away from the plates.

The birefringent liquid crystal is uniaxial. Light polarized parallel to the director sees the extraordinary refractive index n_e; the perpendicular polarization sees the ordinary index n_o. Therefore, for incident light polarized parallel to the microgrooves, the refractive index of the liquid crystal layer will be n_e when the applied electric field strength is below a threshold value. As the amplitude of the voltage increases to the saturation voltage, the molecules will realign themselves until they are perpendicular to the walls. The index of refraction at that point will be n_o. The refractive index will monotonically vary between the two extremes at each intermediate electric field amplitude.

This refractive index modulation shifts the optical phase of light passing through the liquid crystal because of the relationship between phase and index:

$$\phi(n) = \left(\frac{2\pi}{\lambda} L_{LC}\right) n + \phi_0 \qquad (1)$$

where L_{LC} is the physical path length through the liquid crystal, λ is the wavelength of the incident light, and ϕ_0 is an arbitrary constant phase.

The LCPDI is tilted about the horizontal axis to minimize secondary fringes caused by multiple reflections from the glass plates. Anti-reflection coatings on each glass surface can be used in place of this tilt. The LCPDI itself introduces aberrations that must be subtracted from the measured wavefront. This correction will occur automatically if the device is used to measure an initial wavefront subtracted from an altered wavefront such as is the case in fluid studies.

Additional system considerations include temperature control and vibration control. The refractive index of the liquid crystals depends roughly linearly with temperature, with a slope of about $-0.0014°C^{-1}$. To keep Δn within 1% of its value, the temperature of the LCPDI should be maintained within 2°C. Also, although the common-path design makes this interferometer more stable than most, vibrations of the focusing lens, LCPDI, viewing screen and camera should still be minimized.

No attempt was made to increase the data acquisition speed for this work. If fast acquisition is important, the response time of the liquid crystals, normally around 30 ms, can be decreased by rapidly applying a high voltage across the liquid crystal layer before setting the value to the desired voltage. This is known as the transient nematic effect and has been demonstrated to reduce response times down to 1 ms (Perregaux et al. 1987), with response times of around 50 μs theoretically possible (Wu and Wu 1988).

Fig. 1. Liquid crystal point diffraction interferometer filter schematic. Dashed lines indicate reference wave, solid lines indicate object wave

3

Temperature measurement

Fluid scientists are interested in the mechanics of diffusion in the absence of gravity. It is hoped that these studies will lead to improved understanding of the fundamental processes of solidification, thermal and chemical transport, combustion, and turbulence, ultimately leading to better material processing systems, drug delivery, and engine designs. A typical experiment involves the suspension of a bubble or drop in oil. The diffusion across the boundary is studied as an oil property, such as temperature, is changed systematically. A standard piece of experimental equipment is rectangular chamber filled with oil, with two temperature controlled sides. Windows in the other four sides allow observation of the oil. A syringe inserted into a small port allows the injection of a drop of fluorine or a bubble of air into the oil (Rashidnia and Balasubramaniam 1992; Rashidnia 1995).

The LCPDI was used to measure the temperature distribution across the chamber, before the addition of a drop or a bubble. This experiment demonstrates the ability of the LCPDI to measure fluid properties; particularly those of interest to microgravity researchers.

3.1
Experimental apparatus

The experimental equipment is shown schematically in Fig. 2. The chamber used for this experiment was constructed of four Lexan double walls, with inside dimensions $45 \times 45 \times 60$ mm. Double walls are used to reduce heat losses from the sides. Circular fused silica windows were inserted in the center of two opposing walls to provide a high quality viewing port. The windows were 30 mm in diameter, 6 mm thick, and polished to a one-tenth wave finish.

The top and bottom of the chamber were hollow rectangular boxes made from anodized aluminum. A recirculating water bath was connected to each box, allowing water to pass through an external heating or cooling element and then through the box. The temperature control system could maintain a water t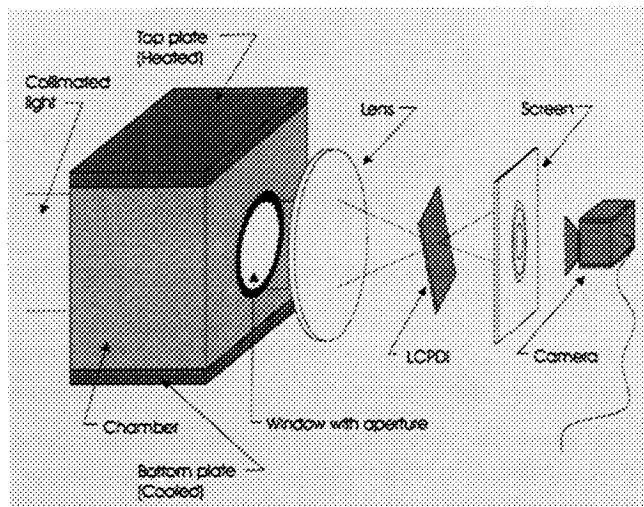emperature stability of 0.01°C. However, the chamber was not insulated, and variations in the ambient room temperature affected the temperature of the chamber side walls. K-type thermocouples in the inner surfaces of the top and bottom chamber walls monitored the temperatures at those surfaces. The electronic readout of these thermocouples had a resolution of 0.1°C. The chamber was filled with 50 centistokes silicone oil. The oil's refractive index at 25°C is 1.4022, and the coefficient of thermal expansion for this index is $\beta = 0.00104$ cc/(cc °C).

A collimated beam of 514.5 nm laser light was passed through the windows of the chamber. The light was generated by an Argon ion laser operated without an etalon, without a prism, and without a constant intensity feedback mechanism. The multiline output intensity was nominally 120 mW, but fluctuated about 20% from this value. Two external prisms and a beam stop were used to select the 514 nm line, and beam steering mirrors brought the light up to the windows' height. Collimating optics were used to produce a 24 mm diameter collimated beam with a power density of nominally 1.5 mW/cm², or 6.8 mW total power. The horizontally polarized light traveled through the test chamber windows. A 16 mm diameter aperture behind the last window sharply truncated the beam. A 100 mm Cooke triplet lens focused the light, forming an $f/6.3$ beam. The LCPDI was oriented with the relaxed liquid crystal molecules lying horizontally; mounted on a 3-axis positioner; and placed just behind the focused spot. A ground glass screen was placed 21 cm behind the LCPDI, and a 50 mm Nikkor lens at $f/5.8$ imaged the interferogram onto a CCD detector array. The array consisted of 768×493 active pixels, each 11.38×13.50 μm.

3.2
Data acquisition

Images from the camera were digitized into a personal computer by a frame grabber. A computer controlled programmable function generator was used to generate the AC voltage for phase stepping. A delay of 7 s was inserted between the time that the voltage was changed and the image was acquired to ensure that the liquid crystals had reached a steady-state orientation. An additional 6 seconds was needed to write the images to the hard drive. The total time for acquiring five phase-stepped interferograms was therefore about 65 s.

In order to measure the temperature distribution across the central portion of the test chamber, two wavefronts were measured. First, five phase-stepped interferograms were recorded to measure the wavefront passing through the chamber with the test fluid at room temperature (isothermal condition). Then the top and bottom chamber plates were set to the desired temperatures and left there for about an hour to allow the oil to reach its steady state condition. The top plate was kept hotter than the bottom plate to allow stable stratification in the presence of gravity. This stable condition was verified continuously observing the interference fringes. Five more phase-stepped interferograms were then recorded to measure the wavefront passing through the heated oil. The difference between these measured wavefronts was then used to determine the temperature distribution across the oil.

The oil temperature distribution along a single line near the center of the chamber was also measured with a thermocouple

Fig. 2. Experimental apparatus for temperature measurement

to verify the LCPDI measurement. The K-type thermocouple was mounted in a 0.8 mm diameter tube that was inserted through a small port in the top of the chamber. The tube was mounted on a traversing stage and scanned from the top to the bottom of the chamber. Temperature readings were taken every millimeter when the probe was within the window area, and every 5 mm when the probe was above and below the window. The temperature was also measured when the probe was at the top and bottom edges of the window. The temperature was displayed on an electronic readout with a resolution of 0.1°C. The calibrated thermocouple had an accuracy better than 0.05°C, but because of the low resolution readout measurement has an accuracy of only 0.1.

3.3
Data processing

A binary mask was created to eliminate information from the interferograms outside the fused silica windows. One of the interferograms was histogram equalized, and then thresholded to produce the mask. Pixels whose value was above the threshold were set to one, and the rest were set to zero. Each interferogram was then multiplied by the mask.

The interferograms were then normalized to compensate for intensity fluctuations caused by not only the rotation of the dye, but also by laser instabilities. A two-dimensional quadratic surface was fit to each unmasked raw interferogram, and the value of each pixel in each interferogram was divided by the value of the corresponding pixel of its quadratic surface (Mercer and Creath 1994b). Two of the normalized, masked interferograms are shown in Fig. 3. One of the five interferograms taken while the chamber was in the isothermal condition is shown in Fig. 3a, and the interferogram shown in Fig. 3b was taken after the top plate was heated.

Each set of five normalized interferograms was used in Hariharan's standard algorithm (Hariharan et al. 1987) to compute the two phase maps. The modulo 2π phase maps were unwrapped, and the aspect ratio of the images was fixed by resampling the x-axis by the ratio of the width and height of the pixels.

The unwrapped, scaled phase maps are shown as wire-mesh plots in Fig. 4, before and after the temperature difference was applied across the chamber. The phase map representing the wavefront passing through the isothermal cell was subtracted from the wavefront measured while the top and bottom plates were set to different temperatures. The difference is shown in Fig. 5.
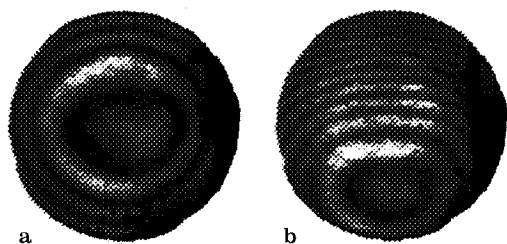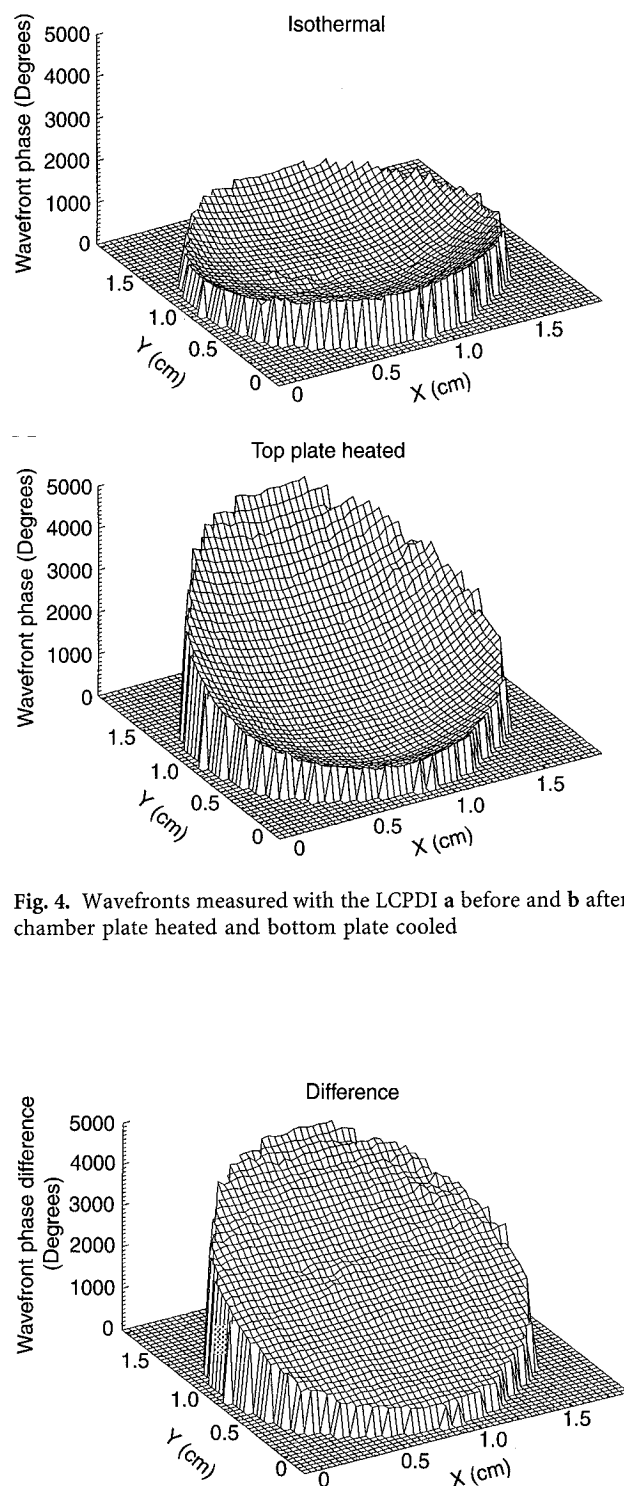

Fig. 4. Wavefronts measured with the LCPDI a before and b after top chamber plate heated and bottom plate cooled

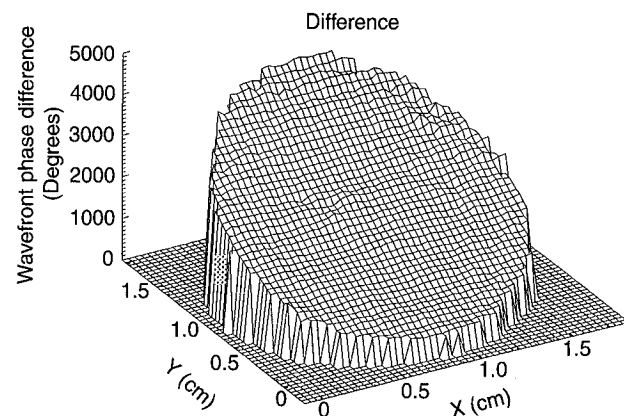**Fig. 5.** Difference between wavefronts measured with isothermal and heated oil chamber

Fig. 3. Normalized masked interferograms taken a before and b after top chamber plate heated and bottom plate cooled

This phase difference occurs because the refractive index of the oil changed with temperature. To determine the temperature distribution that caused this phase difference, the phase difference can be converted to a refractive index distribution, which in turn can be converted to a temperature map. The

following equations were used to perform these conversions:

$$\Delta n = \frac{\lambda}{360°} \frac{\Delta \phi}{L} \qquad (2)$$

$$\frac{dn}{dT} = -\frac{3}{2} \frac{n(n^2-1)}{2n^2+1} \beta \qquad . \qquad (3)$$

$$\Delta T = \frac{\Delta n}{dn/dT} \qquad (4)$$

where L refers to the length of the oil chamber along the optic axis. Equation (3) is taken from Vest (1979). The temperature is therefore proportional to the measured phase.

The isothermal wavefront, the wavefront measured after heating the top plate, and the difference between the two, converted to temperature, are shown as gray-scale images in Fig. 6.
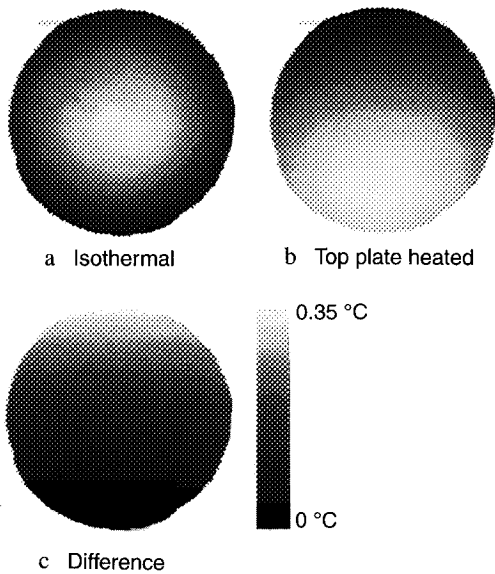

a Isothermal   b Top plate heated

0.35 °C

0 °C

c Difference

Fig. 6. Temperature measurement data **a** wavefront through isothermal chamber; **b** wavefront through heated chamber; **c** difference between the two
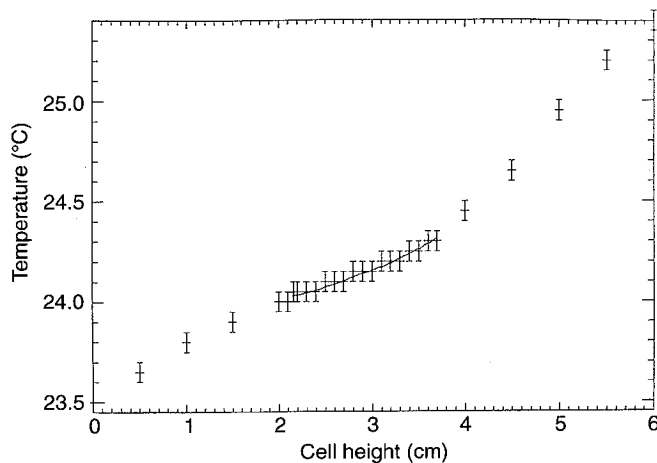

Fig. 7. Plot of temperature across chamber, measured with LCPDI (solid line) and traversing thermocouple (error bars)

The relative temperature difference measured by the LCPDI was converted to an absolute temperature distribution by first determining the column of data corresponding to the axis along which the thermocouple measurements were made. The temperature difference dT was then forced to zero at the bottom of this column by subtracting the measured value of dT at the bottom of the window from the entire LCPDI data set. The temperature measured by the thermocouple at that point was then added to the entire LCPDI data set. The LCPDI curve was then shifted by 0.03 °C to obtain better agreement between the data sets. This shift is well within the ±0.05 °C error bars of the thermocouple data.

The absolute temperature measured by the LCPDI along this column is plotted in Fig. 7, together with the temperature measurements from the traversing thermocouple. As just described, the two curves were forced to intersect at the bottom of the window.

4
Results

The data shown in Fig. 7 indicates excellent agreement between the LCPDI temperature measurement and the thermocouple measurements, certainly to within the 0.1°C resolution of the thermocouple data. The non-linear temperature distribution across the chamber is typical of what has been observed in similar fluid chambers in previous experiments. The thermal gradients are steeper at the top and bottom surfaces of the chamber because heat transfer occurs across the un-insulated walls.

The amount of error in this temperature distribution measured by the LCPDI can be determined by assuming that errors in each of the factors in Eq. (4) are independent from each other. Using the propagation of errors method,

$$\left(\frac{\sigma_T}{T}\right)^2 = \left(\frac{\sigma_\lambda}{\lambda}\right)^2 + \left(\frac{\sigma_\phi}{\phi}\right)^2 + \left(\frac{\sigma_L}{L}\right)^2 + \left(\frac{\sigma_\beta}{\beta}\right)^2 + \left[\frac{2n^4+5n^2-1}{n^2(n^2-1)^2}\right]^2 \sigma_n^2 \qquad (5)$$

If the uncertainty of the phase measurement is 1°, and the uncertainty of each of the other factors is 1%, the uncertainty in the measured temperature is 12.7%. The largest contributor to this uncertainty is the uncertainty in refractive index. If $\sigma n/n$ is 0.25% rather than 1%, the overall uncertainty drops to 3.5%.

This LCPDI technique has been shown to be effective for measuring a thermal gradient of about 0.2°C/cm. This makes the instrument useful for detecting small fluid property variations. As the temperature gradient becomes stronger, the center of the focused spot on the LCPDI will deflect farther from the microsphere. A gradient at least three times as strong as the one demonstrated here should be measurable without difficulty, especially if the LCPDI plate is pre-shifted vertically so that the isothermal interference pattern is shifted towards the hot side of the expected thermal gradient. Nominally linear gradients larger than about 1°C/cm will not be measurable using the technique described herein for two reasons: first, the fringes will become too small for Nyquist detection (Greivenkamp and Bruning 1992), and second, the fringe contrast will be bad because the reference beam intensity will greatly decrease.

Nonetheless, this instrument has been shown to be effective for making sensitive, full-field, fluid temperature measurements. The LCPDI is more accurate and provides more data density than anything currently used in the European (Giglio et al. 1987; Musazzi et al. 1993) or American (Witherow 1987) microgravity programs.

5
Conclusion

The liquid crystal point diffraction interferometer combines the robust, common-path design of the PDI with a simple method of optical phase control. The result is a compact new instrument for the measurement of optical wavefronts that uses phase stepping interferometry for high data density and automatic data reduction.

The LCPDI was used to measure the temperature distribution across a fluid. These demonstrations show that the instrument can accurately measure wavefront differences of interest to fluid scientists. Because the LCPDI introduces errors into the interferograms, it is best used in applications where wavefront differences are of interest. The difference operation will automatically compensate for the induced aberrations. The instrument also has potential for making single measurements provided the initial aberrations can be identified.

References

Aggarwal AK; Kaura SK (1986) Further applications of point diffraction interferometer. J Opt (Paris) 17: 135–138

Bruning JH; Herriott DR; Gallagher JE; Rosenfeld DP; White AD; Brangaccio DJ (1974) Digital wavefront measuring interferometer for testing optical surfaces and lenses. Appl Opt 13: 2693–2703

Giglio M; Paganini E; Perini U (1987) A self-aligning point diffraction interferometer for fluid studies. SPIE Opt Comp Sys 805: 82–86

Greivenkamp JE; Bruning JH (1992) Phase shifting interferometry. In: Optical shop testing (Malacara D, editor), 2nd ed., Chap. 14. New York: Wiley

Hariharan P; Oreb BF; T Eiju T (1987) Digital phase-shifting interferometry: a simple error-compensating phase calculation algorithm. Appl Opt 26: 2504–2506

Linnik VP (1933) Simple interferometer for the investigation of optical systems. Comp Rend de l'Acad des Sci de l'URSS. 1: 208–210

Mercer CR; Creath K (1994a) Liquid crystal point diffraction interferometer. Opt Lett 19: 916–918

Mercer CR; Creath K (1994b) Defocus measurement using a liquid crystal point diffraction interferometer. OSA Opt Fab and Test Wkshp, Tech Dig 13: 293–296

Musazzi S; Perini U; Trespidi F (1993) Point diffraction interferometer for fluids study in microgravity environment. Exp Therm Fluid Sci Sci 6: 49–55

Perregaux AE; Stephany JF; Faucz EC; Hudson RA; Hull VJ; LaKatos AI; Martel RA; Narang R; Richter B (1987) Transient nematic liquid crystal image bar for electrophotographic printers. SID Dig 28: 360

Rashidnia N (1995) Observation of flow and temperature oscillations around a bubble on a solid surface subject to a vertical temperature gradient. AIAA 95–0880

Rashidnia N; Balasubramaniam R (1992) Thermocapillary migration of liquid droplets in a temperature gradient in a density matched system. Exp Fluids 11: 167–174

Smartt RN; Strong J (1972) Point-diffraction interferometer. J Opt Soc Am 62: 737

Speer RJ; Crisp M; Turner D; Mrowka S; Tregidjo K (1979) Grazing incidence interferometry: the use of the Linnik interferometer for testing image-forming reflection systems. Appl Opt 18: 2003–2012

Vest CM (1979) Holographic interferometry. New York: Wiley

Witherow WK (1987) Reconstruction techniques of holograms from Spacelab 3. Appl Opt 26: 2465–2473

Wu S-T; Wu C-S (1988) Small angle relaxation of highly deformed nematic liquid crystals. Appl Phys Lett 53: 1794–1796